

Vulnerabilities in AI-generated Image Detection: The Challenge of Adversarial Attacks

Yunfeng Diao*, Naixin Zhai*, Changtao Miao, Zitong Yu, *Senior Member, IEEE*, Xingxing Wei, Xun Yang†, *Senior Member, IEEE*, Meng Wang, *Fellow, IEEE*

Abstract—Recent advancements in image synthesis, particularly with the advent of GAN and Diffusion models, have amplified public concerns regarding the dissemination of disinformation. To address such concerns, numerous AI-generated Image (AIGI) Detectors have been proposed and achieved promising performance in identifying fake images. However, there still lacks a systematic understanding of the adversarial robustness of AIGI detectors. In this paper, we examine the vulnerability of state-of-the-art AIGI detectors against adversarial attack under white-box and black-box settings, which has been rarely investigated so far. To this end, we propose a new method to attack AIGI detectors. First, inspired by the obvious difference between real images and fake images in the frequency domain, we add perturbations under the frequency domain to push the image away from its original frequency distribution. Second, we explore the full posterior distribution of the surrogate model to further narrow this gap between heterogeneous AIGI detectors, e.g. transferring adversarial examples across CNNs and ViTs. This is achieved by introducing a novel post-train Bayesian strategy that turns a single surrogate into a Bayesian one, capable of simulating diverse victim models using one pre-trained surrogate, without the need for re-training. We name our method as Frequency-based Post-train Bayesian Attack, or FPBA. Through FPBA, we show that adversarial attack is truly a real threat to AIGI detectors, because FPBA can deliver successful black-box attacks across models, generators, defense methods, and even evade cross-generator detection, which is a crucial real-world detection scenario. The code will be shared upon acceptance.

Index Terms—AI-generated Image Detection, Adversarial Examples.

I. INTRODUCTION

The notable progress in generative models, such as GANs [1] and Diffusion models [2], is driving the flourishing development of the image synthesis domain. These generated fake images exhibit realistic-looking, rendering them visually indistinguishable from real images. Moreover, a variety of free and open-source tools facilitates the effortless creation of

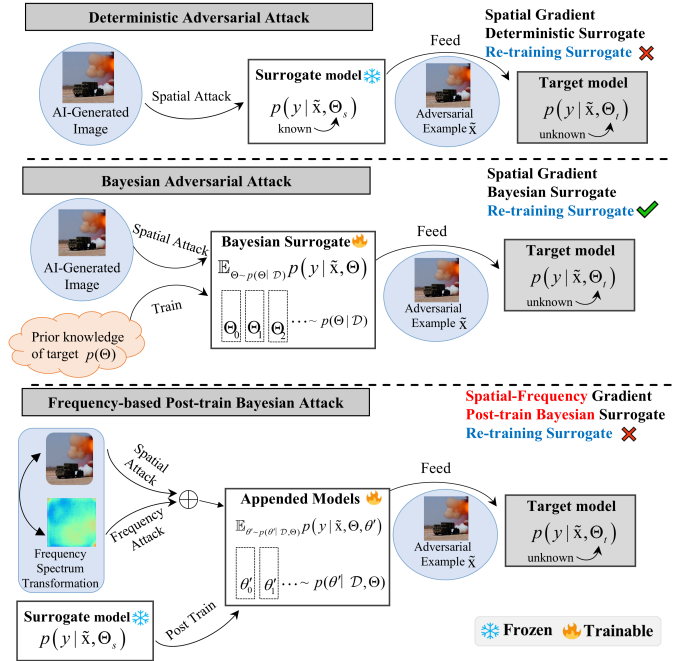


Fig. 1. A high-level illustration of our proposed method.

fake images. However, alongside the benefits, the widespread availability of fake images raises concerns regarding the dissemination of misinformation and fake media news.

Consequently, numerous detectors have been proposed to identify AI-generated images (AIGI). Recent state-of-the-art detectors [3], [4] rely on Deep Neural Networks (DNNs) to classify, achieving significant accuracy performance across multiple datasets and generative models. However, our investigation reveals that AIGI detectors are vulnerable to adversarial examples, capable of misleading detectors by classifying fake images as real. Despite several works [5]–[9] exploring adversarial attacks for GAN-based face forgery detection, we extend this security issue to encompass broader AIGI detection, which has been largely ignored. Unlike face forgery concentrates solely on manipulating or synthesizing faces, often crafted by GANs, AI-generated images span a broader spectrum, generated by a variety of advanced diffusion models and GANs. These images encompass a richer array of semantic content, thus greatly enhancing their potential for disseminating disinformation.

In this paper, we show that AIGI detectors are vulnerable to adversarial attacks. Considering that many works [10], [11] have demonstrated the obvious changes between real and fake images in the frequency domain, we explore the vulnerable

This work was supported in part by the NSF China (No. 62302139) and FRFCU-HFUT (JZ2023HGTA0202, JZ2023HGQA0101).

* Yunfeng Diao and Naixin Zhai contributed equally to this paper.

† Xun Yang is the corresponding author.

Yunfeng Diao and Meng Wang are with the School of Computer Science and Information Engineering, Hefei University of Technology, China (email: diaoyunfeng@hfut.edu.cn, eric.mengwang@gmail.com).

Naixin Zhai and Xun Yang are with the School of Information Science and Technology, University of Science and Technology of China, Hefei, China (email: zhainaxin@mail.ustc.edu.cn, xyang21@ustc.edu.cn); Changtao Miao is with the School of Cyber Science and Technology, University of Science and Technology of China, Hefei, China (e-mail: miaoct@mail.ustc.edu.cn).

Zitong Yu is with the School of Computing and Information Technology, Great Bay University, Dongguan, China (e-mail: yuzitong@gbu.edu.cn).

XingXing Wei is with the Institute of Artificial Intelligence, Beihang University, Beijing, China (e-mail: xxwei@buaa.edu.cn).

region of AIGI detectors in the frequency domain. As illustrated in Fig. 3, the frequency components that different detectors focus on significantly vary from each other. Therefore, we utilize frequency spectrum transformation to uncover diverse substitute models via adding adversarial perturbations in the various frequency transformation domains. Further, Transformer-based detectors have demonstrated outstanding performance in detection AI-generated images [12], but we have observed that there is an obvious gap in adversarial transferability across heterogeneous AIGI detectors e.g. transferring adversarial examples across Convolutional Neural Networks (CNNs) to Visual Transformers (ViTs) (as shown in Table I). To tackle this issue, we propose a post-train Bayesian strategy to conduct a Bayesian treatment on the surrogate model, without the need for re-training the surrogate. In contrast to existing ensemble-based or Bayesian attacks, which involve retraining an ensemble of surrogate models, our post-train Bayesian strategy freezes the pre-trained surrogate and appends tiny extra Bayesian components behind the surrogate, avoiding a heavy memory footprint and speeding up the training process. As a result, we propose a new transferable adversarial attack for general AIGI detection, to add adversarial perturbations in various frequency transformation domains from a post-train Bayesian perspective. We name our method Frequency-based Post-train Bayesian Attack, or FPBA. A high-level illustration of our method and the key differences between our method and the previous method are shown in Fig. 1.

The contributions of this work can be summarized as follows:

- We systemically investigate the adversarial robustness of state-of-the-art AIGI detectors, including standard trained models, defense models, and cross-generated detection within real-world scenarios. We demonstrate adversarial examples are truly a real threat to AIGI detections, and reveal the phenomenon of gradient masking phenomena in AIGI detectors.
- We propose a novel attack against AIGI detection by exploring the vulnerable frequency region in a Bayesian manner. A new post-train Bayesian strategy for attack is proposed to explore the full posterior distribution over the surrogate, without the need for re-training the substitute model.
- We conduct comprehensive experiments on 13 various AIGI detectors, including heterogeneous model architectures and various detection methods. Extensive results demonstrate that our proposed method achieves the highest average attack success rate under white-box and black-box settings, outperforming baseline methods by a big margin.

II. RELATED WORK

AI-Generated Image Detection: The rapid advancement of AI generative technologies, including GANs [1], VAEs [13], and Diffusion models [2], has brought about substantial risks in the dissemination of disinformation. Initially, early VAEs and GANs models were primarily utilized to generate realistic fake face data, leading detection methods [14]–[16], to primarily focus on face forgeries. However, with the emergence of

diffusion models, the scope of generative models has expanded to encompass diverse natural scene objects. Consequently, this expansion presents more significant challenges to detection methods, as they must now address a broader range of forgery types and scenarios.

The primary objective of AIGI detection methods is to discern the authenticity of an image by framing it as a binary classification task, distinguishing between real and fake instances. Data-driven-based approaches [3], [17] have demonstrated promising results on generated data identically distributed. However, their performance significantly degraded when presented with previously unseen generated images. More recently, certain methods [10], [11] focus on analyzing forgery traces in the frequency domain and learning relevant forgery features [18] to enhance the generalization capability of the detection system. In pursuit of these objectives, some methods have been proposed to learn local forgery features [19], [20] in the spatial domain. AIGI fingerprint representations [21] are acquired through the learning of noise patterns. Notably, studies such as [4], [22] have demonstrated the utility of utilizing noise in the frequency domain as a fingerprint for enhancing performance. A sequence of detection methodologies [23] has been progressively investigated, relying on the practice of freezing pre-trained models. These approaches employ parameter-efficient fine-tuning strategies while integrating additional classifiers. For instance, UniFD [24] explores pre-trained vision-language models for AIGI detection, showcasing the effectiveness of leveraging such models in the pursuit of robust forgery detection. Furthermore, other researchers have pursued a comprehensive investigation of generalized forgery features from various perspectives, ranging from diffusion reconstruction error [25], [26], adversarial teacher-student discrepancy-aware framework [27] or diffusion noise [28]. The existing models consistently demonstrate enhancement in detecting AI-generated images. However, their behaviors under adversarial attacks have not been thoroughly examined. Our work is complementary to existing research by making the attempt to systemically evaluate their robustness to adversarial attacks and suggesting potential improvements.

Adversarial Attack: Adversarial attacks aim to generate adversarial examples that can fool the target model into predicting wrongly. The vulnerability of DNNs has sparked significant concerns in many safety-critical fields, including image classification [29], [30], multimedia communication [31] and human activity recognition [32]. Very recently, the adversarial attack against Deepfake detection has drawn attention. Hussain et al. [6] employ gradient sign-based methods [33], [34] to evaluate the adversarial robustness of video Deepfake detectors. Li et al. [35] generate adversarial fake images along the latent face manifold. Carlini et al. [5] and Neekhara et al. [7] investigate the adversarial threat to Deepfake detection under the black-box setting. Jia et al. [9] propose to generate adversarial perturbations in the frequency domain. Hou et al. [8] narrow the feature distribution gap between real and fake images by incorporating natural degradation noise with adversarial perturbations. FakePolisher [36] and TraceEvader [37] improve the untraceability of deepfakes by removing artificial fingerprints. Different from Deepfake tampering the real face

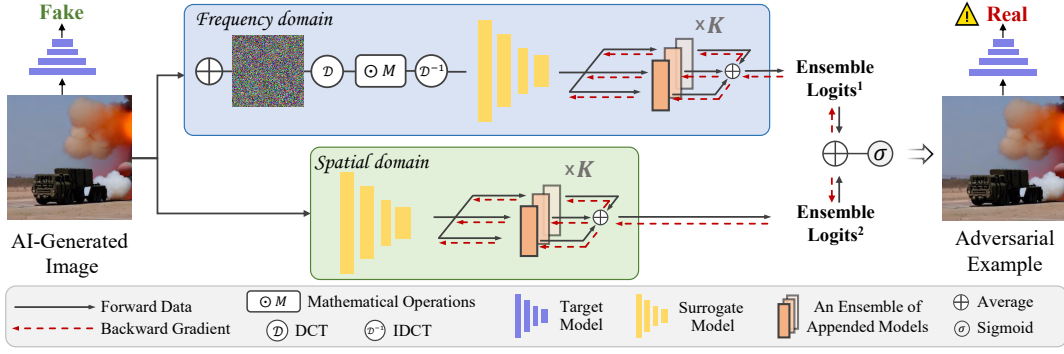


Fig. 2. The workflow of FPBA. We add spatial-frequency adversarial perturbations to AI-generated images in a Bayesian manner, so that they are misclassified as real. DCT and IDCT are discrete cosine transformation and inverse discrete cosine transformation respectively.

images, AI-generated image encompasses a broader range of synthetic images with more diverse semantic content, amplifying their potential for dissemination of disinformation. However, the adversarial robustness of AIGI detection has received little attention. In this paper, we propose a universal attack against both AIGI detectors and Deepfake detectors, and evaluate under the white-box and a more practical black-box setting.

III. METHODOLOGY

A. Preliminaries

Let \mathbf{x} and y represent the original image and its corresponding label. f_{Θ} denotes the AI-generated image detectors. We aim to inject adversarial perturbation into the original image that makes the detector misclassify. Such an adversary problem can be optimized by minimizing the predictive probability, i.e. maximizing the classification loss:

$$\arg \min_{\tilde{\mathbf{x}}} p(y | \tilde{\mathbf{x}}, \Theta) = \arg \max_{\tilde{\mathbf{x}}} L(\tilde{\mathbf{x}}, y, \Theta), \text{ s.t. } \|\delta\|_p \leq \epsilon, \quad (1)$$

where L is the binary cross entropy loss in AI-generated image detection. Adversarial example $\tilde{\mathbf{x}} = \mathbf{x} + \delta$, in which δ is the adversarial perturbation and ϵ is the perturbation budget. Eq. (1) can be performed with iterative gradient-based methods, such as PGD [38] or I-FGSM [33]:

$$\begin{aligned} \tilde{\mathbf{x}}^{i+1} &= \tilde{\mathbf{x}}^i + \alpha \cdot \text{sign}(\nabla L(\tilde{\mathbf{x}}^i, y, \Theta)) \\ &= \tilde{\mathbf{x}}^i - \alpha \cdot \text{sign}(\nabla \log p(y | \tilde{\mathbf{x}}^i, \Theta)). \end{aligned} \quad (2)$$

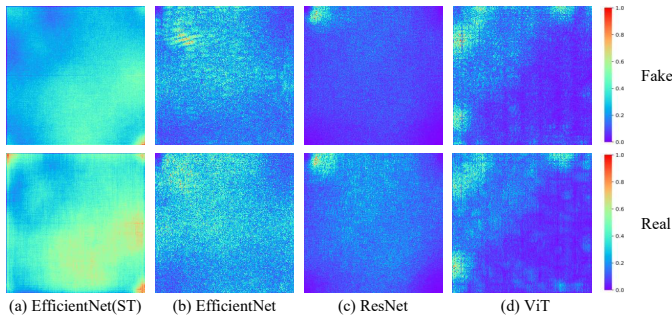


Fig. 3. Visualization of the spectrum saliency map (average 2000 images on GenImage datasets) for real and fake images across different models. (a): the results for conducting frequency spectrum transformation ($N=10$). (b~d): the results for raw images on different models. The color value represents the absolute gradient value of the model loss function after max-min normalization.

B. Frequency-based Analysis and Attacks

Many AIGI detection approaches distinguish between real and fake images via subtle artifacts [3], [4], [21]. While these subtle clues are invisible in the spatial domain, a series of works [10], [11] demonstrate that there are obvious differences between real and fake images in the frequency domain. This inspires us to explore the vulnerable region of AIGI detectors from a frequency perspective. To this end, we first implement discrete cosine transform (DCT) $\mathcal{D}(\cdot)$ to transfer the inputs from the spatial domain to the frequency domain. To investigate the difference between real images and fake images in the frequency domain, we use the spectrum saliency map [39] to visualize the sensitive components of real and fake images across different models:

$$\mathbf{S}_{\Theta} = \frac{\partial J(\mathcal{D}_{\mathcal{I}}(\mathcal{D}(\mathbf{x}), y, \Theta))}{\partial \mathcal{D}(\mathbf{x})}, \quad (3)$$

where $\mathcal{D}_{\mathcal{I}}(\cdot)$ is the inverse discrete cosine transform (IDCT). In a spectrum map, the low-frequency components whose amplitudes are mainly distributed in the upper left corner, and the high-frequency components are located in the lower right corners. As shown in Fig. 3, (1) There are significant differences between synthetic images and real images in the frequency domain. Therefore, moving the image away from its original frequency distribution will make the detectors hardly classify it as the ground-truth class. This observation motivates us to attack under the frequency domain to push the original images away from their ground-truth frequency distribution. (2) Different models usually focus on different frequency components for classifying (Fig. 3(b~d)). This inspires us to conduct random spectrum transformation to stimulate diverse substitute models. Followed by [39], the spectrum transformation $\Gamma(\mathbf{x})$ is defined as:

$$\Gamma(\mathbf{x}) = \mathcal{D}_{\mathcal{I}}(\mathcal{D}(\mathbf{x} + \xi) \odot \mathcal{M}), \quad (4)$$

where $\Gamma(\cdot)$ denotes the random spectrum transformation [39]. \odot is the Hadamard product, ξ is a random noise drawn from an isotropic Gaussian $\mathcal{N}(0, \sigma^2 \mathbf{I})$, and each element of \mathcal{M} is sampled from a Uniform distribution $\mathcal{U}(1-p, 1+p)$. As shown in Fig. 3(a), tuning the spectrum saliency map can cover most of the other models. We hence conduct adversarial attack in the frequency domain via spectrum transformation:

$$\arg \min_{\tilde{\mathbf{x}}} p(y | \Gamma(\tilde{\mathbf{x}}), \Theta), \text{ s.t. } \|\delta\|_p \leq \epsilon. \quad (5)$$

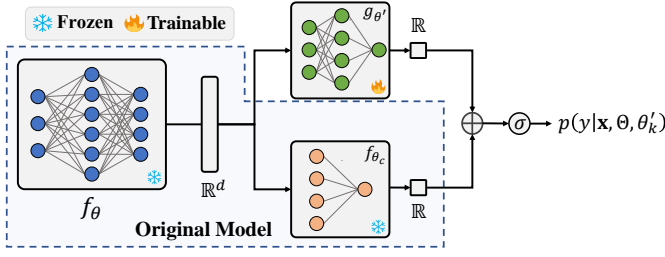


Fig. 4. The architecture of the appended model. σ means the sigmoid layer.

C. Exploring the Surrogate Posterior Space

Although tuning the spectrum transformation in Eq. (5) can simulate different substitute models with a homogeneous architecture [39], it shows limited transferability when applied to heterogeneous architectures, e.g. transferring adversarial examples across ViTs and CNNs. This motivates us to consider the frequency-based attack from a Bayesian perspective, i.e. exploring the full posterior distribution of the surrogate model to further narrow this gap between heterogeneous models. Therefore, we redefine Eq. (5) by minimizing the Bayesian posterior predictive distribution:

$$\begin{aligned} & \arg \min_{\tilde{\mathbf{x}}} p(y | \Gamma(\tilde{\mathbf{x}}), \mathcal{D}) \\ & = \arg \min_{\tilde{\mathbf{x}}} \mathbb{E}_{\Theta \sim p(\Theta | \mathcal{D})} p(y | \Gamma(\tilde{\mathbf{x}}), \Theta), \text{ s.t. } \|\delta\|_p \leq \epsilon, \end{aligned} \quad (6)$$

where $p(\Theta | \mathcal{D}) \propto p(\mathcal{D} | \Theta)p(\Theta)$. \mathcal{D} is the dataset and $p(\Theta)$ is the prior of model weights. Attacking Bayesian Neural Networks (BNNs) rather than a single DNN allows for the output fusion from an ensemble of infinitely many DNNs with diverse predictions, thereby improving adversarial transferability.

1) *Post-train Bayesian Strategy*: However, it is not straightforward to attack AIGI detectors in such a Bayesian manner due to several factors. First, the Bayesian posterior for DNNs is a high dimensional distribution due to a very large number of parameters of DNNs [40]. Hence computing and sampling the posterior distribution is an intractable problem. Albeit feasible for approximate sampling the posterior via variational inference or Markov Chain Monte Carlo (MCMC), it is computationally slow and expensive in such a high dimensional space. Furthermore, to improve the accuracy and generalization of the AIGI detectors, there is a growing inclination to train AIGI detectors on large-scale datasets [12], [41]. From the perspective of end-users, it is not desirable to re-train a surrogate model on large-scale datasets for attack.

Therefore, we propose a *post-train* Bayesian strategy to turn a single surrogate into a Bayesian one, without the need for re-training. The parameters over the pre-trained surrogate are represented as $\Theta = [\theta, \theta_c]$, in which f_θ represents the feature extraction backbone, and f_{θ_c} represents the fully-connected layer network for classification. As shown in Fig. 4, we fix the pre-trained surrogate and append a tiny Bayesian component $g_{\theta'}$ behind the feature extraction backbone f_θ . The new logits can be computed via a skip connection:

$$\text{logits} = g_{\theta'}(f_\theta(\mathbf{x})) + f_{\theta_c}(\mathbf{x}). \quad (7)$$

We choose to apply Bayesian Model Averaging to optimize the appended Bayesian model:

$$\begin{aligned} \mathbb{E}_{\theta' \sim p(\theta' | \mathcal{D}, \Theta)} p(y | \mathbf{x}, \Theta, \theta') & \approx \frac{1}{K} \sum_{k=1}^K p(y | \mathbf{x}, \Theta, \theta'_k), \\ \theta'_k & \sim p(\theta' | \mathcal{D}, \Theta), \end{aligned} \quad (8)$$

where K is the number of appended models. Θ is fixed to avoid re-training. We surprisingly find that adopting a simple MLP layer for appended models works well in all cases, hence training the appended models is much faster than re-training a surrogate. Finally, the frequency-based post-train Bayesian attack can be conducted with iterative gradient-based methods:

$$\tilde{\mathbf{x}}^{i+1} = \tilde{\mathbf{x}}^i - \alpha \cdot \text{sign} \left\{ \frac{1}{K} \sum_{k=1}^K \nabla \log p(y | \Gamma(\tilde{\mathbf{x}}^i), \Theta, \theta'_k) \right\}. \quad (9)$$

2) *Inference on Bayesian Appended Models*: Θ is frozen after pre-training. We use Stochastic Gradient Adaptive Hamiltonian Monte Carlo [42] to sample appended model θ' in each iteration:

$$\begin{aligned} \theta'_{t+1} & = \theta'_t - \sigma^2 \mathbf{C}_{\theta'_t}^{-1/2} \mathbf{h}_{\theta'_t} + \mathbf{N}(0, 2F\sigma^3 \mathbf{C}_{\theta'_t}^{-1} - \sigma^4 \mathbf{I}), \\ \mathbf{C}_{\theta'_t} & \leftarrow (1 - \tau^{-1}) \mathbf{C}_{\theta'_t} + \tau^{-1} \mathbf{h}_{\theta'_t}^2, \end{aligned} \quad (10)$$

where σ represents the step size, F denotes the friction coefficient, \mathbf{h} is the stochastic gradient of the system, \mathbf{N} represents a Normal distribution, \mathbf{I} stands for an identity matrix, \mathbf{C} is a pre-conditioner updated through an exponential moving average, and τ is chosen automatically [42].

D. Hybrid Adversarial Attack

Despite detecting fingerprints fake images in the frequency domain, some works also extract fingerprint features in the spatial domain [3], [21]. We hence incorporate the attack gradient from the frequency domain with the spatial gradient to further improve the adversarial transferability across different domains. Specifically, we define the hybrid attack as:

$$\tilde{\mathbf{x}}^{i+1} = \tilde{\mathbf{x}}^i - \alpha \cdot \text{sign} \left\{ \frac{1}{K} \sum_{k=1}^K (g_k^i + d_k^i) \right\}, \quad (11)$$

$$g_k^i = \frac{1}{N} \sum_{n=1}^N \nabla \log p(y | \Gamma(\tilde{\mathbf{x}}_{n-1}^i), \Theta, \theta'_k), \tilde{\mathbf{x}}_0^i = \tilde{\mathbf{x}}^i, \quad (12)$$

$$d_k^i = \nabla \log p(y | \tilde{\mathbf{x}}^i, \Theta, \theta'_k), \quad (13)$$

where g_k^i and d_k^i are the gradients computed in the frequency domain and spatial domain respectively. For frequency gradient, we conduct random spectrum transformation with N times to get more diverse spectrums. Our proposed method leverages both spatial attack gradients and frequency attack gradients in a Bayesian manner, aiming to further narrow the discrepancy between surrogate models and victim models. The complete algorithm of our method is presented in Algorithm 1. An overview illustration of FPBA is shown in Fig. 2.

Algorithm 1: Inference on FPBA

Input: \mathbf{x} : training data; N_{tra} : the number of training iterations; $M_{\theta'}$: sampling iterations for θ' ; Θ : parameters over pre-trained surrogate model; $\{\theta'_1, \dots, \theta'_K\}$: parameters over appended models; K : the number of appended models;

Output: The adversarial example $\tilde{\mathbf{x}}$;

// Post-train Bayesian Optimization

Randomly initialize $\{\theta'_1, \dots, \theta'_K\}$;

for $j = 1$ **to** N_{tra} **do**

for $n = 1$ **to** K **do**

 Randomly sample a mini-batch data $\{\mathbf{x}, y\}_j$;

 Compute $\mathbf{h}_{\theta'_k} = \frac{\partial \log p(y|\mathbf{x}, \Theta, \theta'_k)}{\partial \theta'_k}$;

for $t = 1$ **to** $M_{\theta'}$ **do**

 Update θ'_k with $\mathbf{h}_{\theta'_k}$ via Eq. (10);

end

end

end

return $\{\theta'_1, \dots, \theta'_K\}$;

// Frequency-based Post-train Bayesian Attack

$\tilde{\mathbf{x}}^0 = \mathbf{x}$;

for $i = 1$ **to** I **do**

for $n = 1$ **to** N **do**

 Get spectrum transformation output $\Gamma(\tilde{\mathbf{x}}^i)$ using Eq. (4);

end

for $k = 1$ **to** K **do**

 Average frequency gradient g_k using Eq. (12);

 Calculate spatial gradient d_k using Eq. (13);

end

 Sample $\tilde{\mathbf{x}}^{i+1}$ from $\tilde{\mathbf{x}}^i$ via Eq. (11);

end

return $\tilde{\mathbf{x}}$;

IV. EXPERIMENTS

A. Experimental Settings

Datasets: We choose three generated image datasets created by a wide range of generative models, across AIGI detection and Deepfake detection. Synthetic LSUN is a commonly used dataset proposed by CNNSpot [3], containing 360k real images from LSUN and 360k fake images generated by ProGAN [43]. GenImage [12] is a recently proposed large-scale dataset, containing 1331k real images and 1350k fake images generated by eight generative models. Following the protocol in [12], we employ a subset of GenImage collecting 162k real images from Imagenet [44] and 162k Stable Diffusion(SD) V1.4 [45] generated images for training. The images generated by the other generators are used for testing in Section IV-C2. To verify our proposed attack is a universal threat across AIGI and Deepfake detection, we also employ the synthetic FFHQ face dataset proposed by [46]. The Deepfake dataset consists of 50k real face images from FFHQ [47] and 50k generated face images generated by StyleGAN2 [47]. After training, we collect only the correctly classified testing samples for attack in evaluation.

Evaluated Models: We extensively evaluate the transferability of adversarial examples by 13 state-of-the-art AIGI detectors, including heterogeneous model architectures and various detection methods. For evaluating on different model architectures, we choose CNN-based detectors CNNSpot [3], MobileNet [48], EfficientNet [49] and DenseNet [50], and ViT-based detectors Vision Transformer(ViT) [51] and Swin-Transformer(Swin-ViT) [52]. For evaluating on various detection methods, we use frequency-based detectors DCTA [11] and Spec [18], gradient-based detectors LGrad [23], CLIP-based detectors UnivFD [24], and diffusion-based detectors DNF [28]. In addition, LNP [22] extracts the noise pattern of images and GramNet [53] learns the global texture representation. We also consider them as victim models.

Compared Methods: We adopt gradient-based methods, I-FGSM [33], PGD [38], MI [54] and frequency-based methods S²I [39], SSAH [55] and ensemble-based methods ENS [54] and SVRE [56]. Because attacks against Deepfake detectors are the most similar adversaries to ours, we also consider state-of-the-art Deepfake detection attacks Fakepolisher [36] and TraceEvader [37] as baselines. Fakepolisher and TraceEvader remove the Deepfake traces and we follow their default settings. For other iterative attacks, we run 10 iterations with step size $\alpha = 2/255$ under l_∞ perturbation budget of $8/255$ for all these attacks.

Implementation Details: For MobileNet, EfficientNet, DenseNet, ViT and Swin-Transformer(Swin-ViT), we train them following the default setting in CNNSpot [3]. Specifically, we choose classifiers pre-trained on ImageNet, and train them with Adam optimizer using Binary Cross-Entropy loss with an initial learning rate of 0.0001. For a fair evaluation, we follow the same data augmentation strategy used in CNNSpot [3] to improve the models' generalization and robustness. Before cropping, images are blurred with $\sigma \sim \text{Uniform}[0, 3]$ with 10% probability, and JPEG-ed with 10% probability. We transformed images to 224 pixels on LSUN(ProGAN) and GenImage(SD) datasets following CNNSpot [3]. On the FFHQ (StyleGAN2) dataset we resized images to 224 pixels to ensure the integrity of the real/fake faces. Subsequently, we apply ImageNet normalization across three datasets. For other AIGI detectors, we use the pre-trained model from their official code. For post-train Bayesian optimization, we follow the default setting in [57]. Although BNNs theoretically necessitate sampling numerous for inference, in practice, we find the number of models $K = 3$ is adequate. Opting for a larger number of appended models escalates computational overhead; thus, we opt for $K = 3$. For frequency-based attack, we set the tuning factor $\rho = 0.5$ for \mathcal{M} , the standard deviation σ of ξ is set to the value of ϵ , following [39]. All experiments were conducted on 4 NVIDIA GeForce RTX 3090s.

B. Attack on Spatial-based and Frequency-based Detectors

We report the attack performance against spatial-based and frequency-based detectors in Table I. Under the white-box setting, our proposed method FPBA achieves the highest attack success rate in all cases, and outperforms other competitive methods. Specifically, FPBA gets an average white-box success rate across different datasets and models as high as 99.6%,

TABLE I

THE ATTACK SUCCESS RATE(%) ON CNN-BASED, ViT-BASED AND FREQUENCY-BASED MODELS ON THE SYNTHETIC LSUN AND GENIMAGE SUBSET. “AVERAGE” WAS CALCULATED AS THE AVERAGE TRANSFER SUCCESS RATE OVER ALL VICTIM MODELS EXCEPT FOR THE SURROGATE MODEL. WE MARK THE WHITE-BOX ATTACK RESULTS IN GRAY, AND BLACK-BOX ATTACK RESULTS ARE NOT MARKED WITH COLORS.

	Surrogate Model	Attack Methods	CNNSpot	DenseNet	EfficientNet	MobileNet	Spec	DCTA	ViT	Swin	Average
LSUN (ProGAN)	CNNSpot	IFGSM	52.1	51.3	24.6	48.4	17.7	48.0	35.2	46.2	38.7
		MIFGSM	52.1	51.5	27.9	47.6	26.1	49.8	37.5	42.7	40.4
		PGD	78.3	77.6	49.4	73.0	25.6	47.6	41.0	70.2	54.9
		S ² I	97.8	86.4	61.5	78.6	20.5	40.8	11.7	74.5	53.4
		SSAH	97.8	2.5	1.3	3.0	0.8	1.0	1.0	0.7	1.4
		FPBA(Ours)	98.9	98.0	76.4	95.9	19.8	48.0	51.5	94.8	69.2
	MobileNet	IFGSM	14.3	17.8	22.4	75.4	17.2	34.9	9.2	18.4	19.2
		MIFGSM	23.8	23.9	28.6	75.4	19.6	42.0	15.5	24.8	25.5
		PGD	20.3	26.0	20.6	97.6	25.0	40.4	9.7	29.9	24.6
		S ² I	14.4	17.5	34.7	97.8	16.3	25.4	4.3	14.6	18.2
		SSAH	0.6	1.0	1.5	99.2	0.5	0.8	1.0	1.1	0.9
		FPBA(Ours)	32.2	40.4	51.7	99.6	22.6	36.4	12.3	44.6	34.3
GenImage(SD)	CNNSpot	IFGSM	78.3	71.5	30.9	34.0	27.1	28.3	11.0	27.8	32.9
		MIFGSM	78.3	75.3	30.1	35.8	27.8	28.3	15.0	28.2	34.4
		PGD	99.3	88.0	48.5	52.2	48.6	49.9	15.4	48.1	50.1
		S ² I	98.0	91.0	66.8	64.7	36.7	50.1	16.9	53.0	54.2
		SSAH	94.8	5.4	0.5	1.1	0.6	3.6	0.7	0.3	1.7
		FPBA(Ours)	100	96.6	59.4	67.3	47.9	49.8	21.1	51.2	56.2
	MobileNet	IFGSM	9.0	8.9	8.9	58.9	9.1	9.1	4.4	8.5	8.3
		MIFGSM	9.7	9.2	8.9	59.0	9.5	9.0	5.9	8.8	8.7
		PGD	42.3	39.9	36.4	97.1	48.4	49.8	14.2	40.0	38.7
		S ² I	35.6	33.1	26.8	78.7	24.1	43.4	6.2	28.0	28.2
		SSAH	1.1	2.0	0.6	96.7	0.5	1.9	1.2	2.2	1.4
		FPBA(Ours)	49.7	46.8	44.0	100	44.1	49.4	16.6	45.0	42.2

TABLE II

THE ATTACK SUCCESS RATE(%) COMPARED WITH ATTACKS AGAINST DEEFAKE DETECTORS(ONLY FAKE ASR). DENNET, EFFNET, MOBNET REFERS TO DENSENET, EFFICIENTNET, MOBILENET RESPECTIVELY.

Datasets	Attack	CNNSpot	DenNet	EffNet	MobNet	ViT	Swin	Ave.
LSUN (ProGAN)	FakePolisher	94.5	98.3	71.6	88.6	15.1	99.5	77.9
	TraceEvader	0.6	1.3	4.5	4.8	8.10	11.4	1.9
	FPBA	100.0	100.0	98.2	99.5	38.6	99.9	89.4
GenImage (SD)	FakePolisher	93.5	93.2	12.2	95.5	33.5	97.6	70.9
	TraceEvader	46.1	34.3	9.4	37.0	15.2	44.3	31.1
	FPBA	100.0	99.7	97.7	98.9	42.1	97.9	89.4

while S²I, PGD, IFGSM and MIFGSM only have 93.1%, 93.1%, 66.2% and 66.2%. Although SSAH has a relatively high white-box success rate (97.7%), it fails to transfer the adversarial examples to black-box models. Under the black-box setting, FPBA still achieves the highest average transfer success rate of 50.5%, surpassing the IFGSM, MIFGSM, PGD, S²I and SSAH by a big margin of 25.7%, 23.3%, 8.4%, 11.9% and 49.1%. Note that our proposed FPBA significantly outperforms the SOTA frequency-based attack S²I and SSAH, demonstrating that FPBA is a stronger frequency-based attack against AIGI detectors.

1) Comparison with Attacks against Deepfake Detectors:

Attacks against Deepfake detectors are similar to our attacks. However, Deepfake mainly manipulating or synthesizing faces, often crafted by GANs. In contrast, AIGI detectors identify any type of visual content generated by diverse techniques, such as GANs, diffusion models, and autoregressive models. The content includes humans, non-human entities, abstract art, landscapes, and more. These differences make it challenging to transfer attacks from DeepFake detectors to AIGI detectors. For example, techniques like searching for adversarial

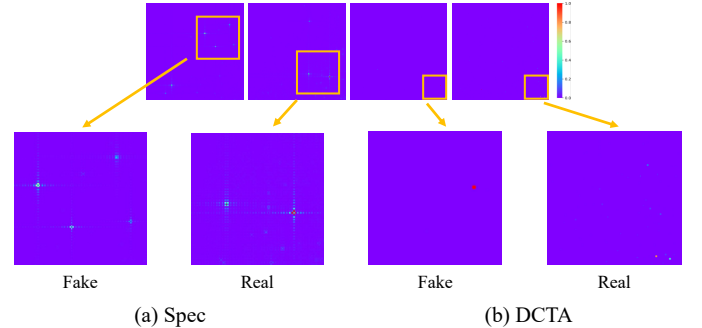


Fig. 5. Visualization of the sensitive frequency components of real and fake images (average 1000 images on LSUN/ProGAN datasets) for frequency-based models. The frequency components of frequency-based models are highly sparse in comparison with spatial-based models. The color value represents the absolute gradient value of the model loss function after max-min normalization.

points on the face manifold [35] or removing facial forgery traces [36], [37] may not be applicable for AIGI detectors. To demonstrate this, we compare with FakePolisher [36] and TraceEvader [37], which are both the SOTA attacks for Deepfake detection. Because FakePolisher and TraceEvader are designed for removing forgery traces, we follow their default setting to only report the attack success rate on fake images. As shown in Table II, FPBA significantly outperforms FakePolisher and TraceEvader on both AIGI datasets. Although FakePolisher performs better than TraceEvader, but the former largely reduces the image quality, which is very visible and raises suspicion (Fig. 7). We suspect this is because FakePolisher has only learned the face manifold, limiting its ability to reconstruct fine-grained details in AIGI images.

TABLE III

THE ATTACK SUCCESS RATE(%) COMPARED WITH ENSEMBLE ATTACK METHODS ON SYNTHETIC LSUN DATASETS. ¹ MEANS SETTING (1), I.E. TAKING AN ENSEMBLE OF CNNSPOT, MOBILENET, AND EFFICIENTNET; ² MEANS SETTING (2), I.E. TAKING AN ENSEMBLE OF CNNSPOT, MOBILENET AND ViT; ³ MEANS SETTING (3), I.E. TAKING AN ENSEMBLE OF CNNSPOT, DCTA AND ViT. ⁴ MEANS ONLY USING CNNSPOT AS SURROGATE MODEL.

Attack	CNNSpot	DenNet	EffNet	MobNet	Spec	DCTA	ViT	Swin	Ave
ENS ¹	55.9	45.4	69.9	76.2	16.8	42.9	23.3	43.7	34.4
SVRE ¹	63.7	64.5	75.5	72.9	10.3	30.4	28.6	64.2	39.6
ENS ²	57.3	58.6	54.1	92.8	19.5	38.5	77.9	59.7	46.0
SVRE ²	77.7	77.9	76.4	97.8	13.9	33.6	70.1	78.1	56.0
ENS ³	9.7	6.3	4.8	10.1	37.0	72.9	20.6	5.5	12.7
SVRE ³	22.6	12.9	8.1	13.2	29.4	87.0	24.0	9.6	14.6
FPBA⁴	98.9	98.0	76.4	95.9	19.8	48.0	51.5	94.8	69.2

TABLE IV

TRANSFER-BASED ATTACK AGAINST SOTA DETECTORS ON SYNTHEIC LSUN (PROGAN) DATASETS. THE SURROGATE MODEL IS CHOSEN AS CNNSPOT [3].

Attack	GramNet	LGrad	LNP	UnivFD	DNF	Ave
MIFGSM	9.7	6.6	38.5	24.2	46.7	25.1
PGD	67.7	50.2	47.4	11.5	48.3	45.0
S ² I	49.1	49.1	28.3	8.3	43.0	35.6
FPBA	87.8	50.2	39.5	16.6	49.8	48.9

TABLE V

BENIGN ACCURACY OF MODELS TRAINED ON SD V1.4 AND EVALUATED ON DIFFERENT GENERATED DATA. ‘REAL/FAKE’ MEANS THE ACCURACY(%) ON EVALUATING REAL/FAKE TESTING DATA.

Detector	Acc	Midj.	SDv1.4	SDv1.5	ADM	Wukong	BigGAN	Ave
Swin-ViT	All	60.5	100.0	99.9	50.8	99.7	50.0	76.8
	Real	100.0	100.0	100.0	100.0	100.0	99.9	100.0
	Fake	21.0	100.0	99.9	1.5	99.3	0.1	53.6
CNNSpot	All	62.0	99.6	99.5	50.3	97.9	49.8	76.5
	Real	99.4	99.6	99.6	99.5	99.6	99.4	99.5
	Fake	24.7	99.6	99.4	1.2	96.1	0.2	53.5
ViT	All	58.4	99.5	99.3	50.2	96.0	50.2	75.6
	Real	99.5	99.6	99.5	99.5	99.5	99.3	99.5
	Fake	17.4	99.3	99.1	0.9	92.4	1.1	51.7

2) *Comparison with Ensemble-based Attacks:* Considering that FPBA attacks an ensemble of appended models, we thus compare it with state-of-the-art ensemble-based methods ENS [54] and SVRE [56], i.e. utilizing an ensemble of surrogate models to generate adversarial examples. To examine the impact of different surrogate combinations(CNN-based vs. ViT-based vs. Frequency-based detectors), we conduct an ablation study for ENSEMBLE and SVRE to investigate their impacts in 3 settings, including (1) taking CNNs as ensemble surrogates (CNNSpot, MobileNet, EfficientNet); (2) taking CNNs and ViTs as ensemble surrogates (CNNSpot, MobileNet, ViT); (3) taking CNNs, ViTs and frequency-based detectors as ensemble surrogates (CNNSpot, DCTA, ViT). Although we can also use more than one architecture for our method, we only use CNNSpot as the surrogate architecture to verify the universal transferability across heterogeneous models. We report the results in Table III. First, compared with setting (1), heterogeneous model ensemble in setting (2) enhances the transferability of ENSEMBLE and SVRE across ViT-based and CNN-based models, while a more comprehensive ensemble in setting (3) decreases the transferable performance except for the frequency-based detectors. We speculate that there are significant differences in the classification boundaries between frequency-based and spatial-based detectors, thus averaging the ensemble outputs might reduce the original attack strength crafted by a single surrogate. Second, FPBA solely on CNNSpot still achieves competitive results in comparison

TABLE VI

THE ATTACK SUCCESS RATE (ASR) OF CROSS-GENERATOR IMAGE DETECTION ON DIFFERENT GENERATED SUBSETS. THE SURROGATE MODEL IS CHOSEN AS SWIN-ViT.

Victim	Midj.	SDv1.4	SDv1.5	ADM	Wukong	BigGAN	Ave
Swin-ViT	97.6	97.4	97.7	96.2	96.9	97.1	97.1
CNNSpot	22.9	44.2	44.8	5.0	44.9	6.2	28.0
ViT	19.9	14.5	16.6	3.3	20.1	2.1	12.7

TABLE VII

THE ATTACK SUCCESS RATE (ASR) IS REPORTED ON REAL IMAGES AND FAKE IMAGES RESPECTIVELY. THE SURROGATE MODEL IS CHOSEN AS SWIN-ViT.

Victim	ASR	Midj.	SDv1.4	SDv1.5	ADM	Wukong	BigGAN	Ave
Swin-ViT	Real	94.9	96.4	96.2	96.0	96.0	97.0	95.9
	Fake	96.5	98.3	98.7	100.0	97.9	100.0	98.3
CNNSpot	Real	3.0	3.4	2.9	2.0	3.6	4.6	3.2
	Fake	100.0	85.1	86.9	100.0	86.3	100.0	93.0
ViT	Real	0.1	0.0	0.3	0.3	0.4	0.4	0.3
	Fake	96.1	29.0	32.9	100.0	39.8	100.0	66.3

with ensemble methods. Somewhat surprisingly, the black-box results on FPBA even outperform white-box results on ENSEMBLE and SVRE in some cases. For instance, the adversarial example only generated by CNNSpot with FPBA get success rate of 76.4% on EfficientNet, which is higher than ENSEMBLE¹ and SVRE¹ generated by an ensemble of CNNSpot, EfficientNet and MobileNet. This demonstrates our proposed method can approximate the true posterior distribution, in which different victim models can be sampled from the posterior.

3) *Evaluation on Frequency-based Detectors:* Although FPBA has the best average success rate, we find that the attack results are usually not the best on frequency-based models. To further investigate the reason, we plot the spectrum saliency map of frequency-based detectors using Eq. (3) in Fig. 5. Unlike spatial-based detectors, which rely on numerous frequency components to make decisions (see Fig. 3), the frequency components focused on in frequency-based models are very sparse. Therefore, the gradient information available from the spatial domain is much richer compared to the frequency domain. Nevertheless, FPBA still gets an top-2 average transfer success rate of 43.1% against frequency-based detectors, which is only slightly lower 1.5% than PGD, and much higher 3.3%, 15.8% and 17.6% than S²I, MIFGSM and IFGSM respectively.

C. Evaluation on Diverse Detection Strategies

1) *Attack Various SOTA Detection Methods:* Except for detecting in spatial and frequency domain using different backbone models, recent AIGI detectors utilize different latent feature representations to identify synthetic artifacts. Specifically, GramNet [53] extracts the global texture representation; UnivFD [24] captures semantic feature using pre-trained CLIP [58]; LNP [22] extracts the noise pattern of images; LGrad [23] extract gradient information through a pre-trained model and DNF [28] leverages diffusion noise features, extracting them through an inverse diffusion process [2]. These significant differences among various detection methods present challenges for the transferability of adversarial examples. To illustrate this, we examine the adversarial transferability of various detection methods and present the results in Table IV. Overall, the transfer success rate is relatively low compared to the results in Table I, suggesting that the

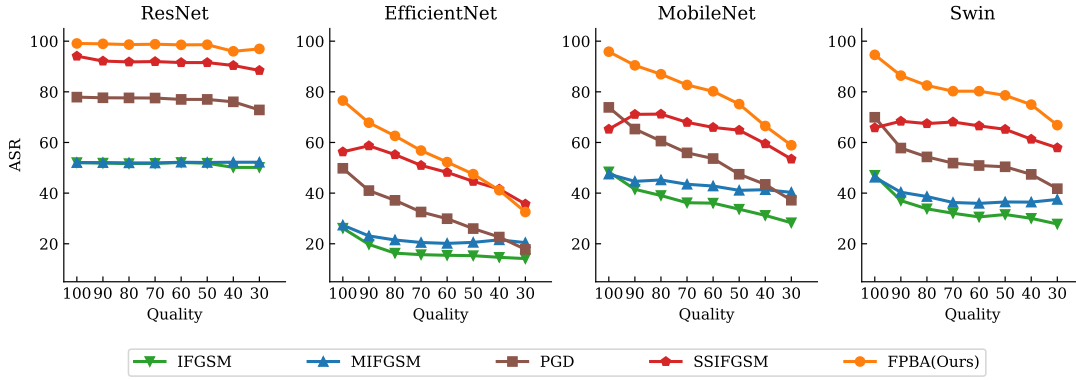


Fig. 6. Attack performance on ResNet, Efficient, MobileNet and Swin against JPEG compression on LSUN(ProGAN) dataset. Adversarial samples are crafted from ResNet.

distinct characteristics of detection methods limit adversarial transferability on each other. Nevertheless, FPBA still give the best adversarial transferability.

2) *Attack Cross-Generator Image Detection*: One important real-world detection problem is cross-generator image detection, i.e. identifying fake images generated by unseen generative models. We hence evaluate the robustness of cross-generator image detection to investigate whether adversarial examples are a real threat to AIGI detection. We train the detectors on images generated by SD v1.4 [45] and assess their robustness against adversarial examples, in which the adversarial perturbations are added to the images generated by Midjourney [59], SD V1.4 [45], SD V1.5 [45], ADM [60], Wukong [61] and BigGAN [62]. Because Swin-ViT achieves the SOTA results on different subsets [12], we use it as the surrogate model.

The benign accuracy and attack performance on unseen source data are reported in Table V and Table VI respectively. First, the attack under the white-box setting achieves almost 100% success rate. Second, the transfer success rate is positively correlated to the accuracy on unseen source data. The Midjourney, SD v1.4&v1.5 and Wukong subsets have relatively high accuracy, their corresponding transfer attack success is also relatively high. In contrast, the binary classification accuracy drops to 50% on ADM and BigGAN subsets, the corresponding adversarial transferability is also limited on them. By looking closely at the accuracy/ASR on real images and fake images (Table V, Table VII), we find detectors fail to distinguish fake images on ADM and BigGAN, which means without a good gradient can be followed to misclassify the real image as fake label under the attack. Therefore, we suggest robustness evaluation of cross-generator image detection should be conducted on the test subset with high accuracy as evaluating on the low-accuracy subset is futile.

D. Attack Performance against Compression in Real Scenarios

In real-world scenarios, images are often compressed during propagation, which may also distort adversarial noise patterns. Therefore, ensuring the effectiveness of adversarial attacks on compressed images is crucial for simulating real-world scenarios. To this end, we perform JPEG compression with quality

TABLE VIII
DEFENSE MODELS (BLUR+JPEG) AGAINST ADVERSARIAL ATTACK ON PROGAN DATASET. BLUR+JPEG(0.1) AND BLUR+JPEG(0.5) REPRESENTED THAT IMAGES ARE BLURRED AND JPEG-ED WITH 10% AND 50% PROBABILITY RESPECTIVELY. WE REPORT THE ATTACK SUCCESS RATE(%).

	Swin-ViT	
	Blur+JPEG(0.1)	Blur+JPEG(0.5)
IFGSM	98.8	86.6(-12.2)
MIFGSM	98.3	92.7(-5.6)
PGD	99.3	87.3(-12)
S ² I	100.0	80.9(-19.1)
FPBA	100.0	99.2(-0.8)

factors of 30, 40, 50, 60, 70, 80, 90 and 100 to the tested images. We evaluate the degradation in attack performance using four models: ResNet-50, EfficientNet, MobileNet and Swin Transformer. All adversarial samples are crafted from ResNet-50. The results are reported in Fig. 6. For white-box attacks on ResNet, JPEG compression has a negligible effect on the attack success rate across different attack methods, maintaining top-1 attack performance. For transfer-based attacks, the attack strength on victim models decreases as the quality factor decreases. However, FPBA consistently maintains the highest attack success rate, demonstrating the effectiveness of our attack method under the real-world scenarios.

1) *Attack Defense Models*: Furthermore, we evaluate FPBA on attacking defense models. We first employ adversarial training [38] for evaluation, which is the most popular defense baseline. However, according to our preliminary experiments (reported in the supplementary material), the training process of adversarial training fails to converge, which shows adversarial training is not a reliable way for evaluating attacks on AIGI detection. Considering that AIGI detection typically [3] uses JPEG compression and Gaussian blurring as data preprocessing during training to improve their robustness, we follow the suggestions from [3], [12] to utilize Gaussian blurring and JPEG compression as a defense. As shown in Table VIII, existing attack methods all suffer from performance degradation as the probability of using Gaussian blurring and JPEG compression increases during training, while FPBA still contains a high attack success rate, which validates its effectiveness.

TABLE IX

THE ATTACK SUCCESS RATE(%) ON CNN-BASED, ViT-BASED AND FREQUENCY-BASED MODELS ON THE SYNTHETIC FFHQ DATASETS. “AVERAGE” WAS CALCULATED AS THE AVERAGE TRANSFER SUCCESS RATE OVER ALL VICTIM MODELS EXCEPT FOR THE SURROGATE MODEL. WE MARK THE WHITE-BOX ATTACK RESULTS IN GRAY, AND BLACK-BOX ATTACK RESULTS ARE NOT MARKED WITH COLORS.

	Surrogate Model	Attack Methods	CNNSpot	DenseNet	EfficientNet	MobileNet	Spec	DCTA	ViT	Swin	Average
FFHQ (Style GAN)	CNNSpot	IFGSM	67.5	67.5	55.3	67.5	28.9	32.5	16.2	17.5	40.8
		MIFGSM	67.5	67.5	54.9	67.6	28.8	32.6	20.7	17.9	41.4
		PGD	100	100	88.6	99.9	49.9	50	40.7	50.0	68.4
		S ² I	100	100	77.7	90.1	46.7	52.9	37.6	55.8	65.8
		SSAH	99.0	54.5	44.1	41.0	2.6	7.2	1.0	4.2	22.1
		FPBA(Ours)	100	100	86.8	100	49.4	49.6	43.1	50.9	68.5
	MobileNet	IFGSM	10.7	12.7	23.8	60.4	24.5	28.4	7.3	10.2	16.8
		MIFGSM	10.3	12.6	23.2	60.4	25.4	28.7	9.1	10.2	17.1
		PGD	49.8	50.2	57.5	100	49.7	49.8	38.8	49.8	49.4
		S ² I	82.8	86.7	78.5	100	51.4	51.8	28.9	49.7	61.4
		SSAH	1.9	36.4	43.7	98.5	2.0	6.2	0.8	2.4	13.3
		FPBA(Ours)	51.2	55.2	66.6	100	50.3	49.9	39.4	49.8	51.8

TABLE X

THE VISUAL QUALITY OF DIFFERENT ATTACK SAMPLES IN TERMS OF THE AVERAGE MSE, PSNR AND SSIM SCORES.

Attack	MSE↓	PSNR(db)↑	SSIM↑
PGD	30.00	33.51	0.88
FakePolisher	34.63	32.92	0.88
FPBA(Ours)	16.08	36.26	0.94

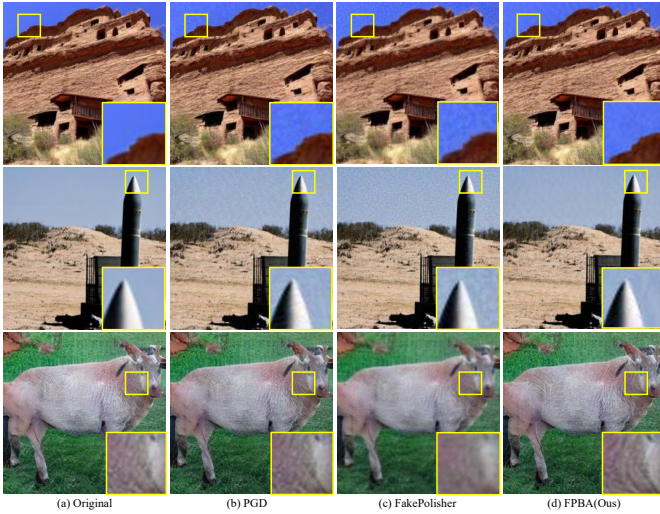


Fig. 7. Visual comparison with PGD. (a): the original image generated by diffusion models. (b): adversarial examples crafted by PGD. (c): the original image generated by FakePolisher. (d): adversarial examples crafted by FPBA. The image quality of the adversarial example crafted by our method is much closer to the original image.

E. Visual Quality Analysis

To demonstrate the superior image quality achieved by our method, we conduct both qualitative and quantitative assessments. We first visualize adversarial examples generated by PGD, FakePolisher and our proposed FPBA in Fig. 7. Adversarial examples from PGD and FakePolisher show noticeable noise patterns upon zooming in. In addition, the fine-grained details of object generated by FakePolisher are blurred, which is very obvious in the goat’s texture and outline in its adversarial images. In contrast, FPBA generate more natural-looking adversarial examples. Further, we also report the quantitative results using common metrics for image quality assessment including MSE, PSNR(db) and SSIM. As reported in Table X, FPBA outperforms other baselines across

all quality assessment by a large margin. This suggests that FPBA adding adversarial noise in the frequency-domain, rather than directly in the spatial domain, is more imperceptible to observers.

F. Additional Performance Analysis

1) *The Phenomenon of Gradient Masking in AIGI Detectors*: In Table I, we find that the attack results of MIFGSM are similar to IFGSM, and significantly lower than PGD, in contrast to the common belief that adversarial examples generated by momentum iterative methods have higher success rate [54]. It indicates the possibility of gradient masking [63]. To investigate whether AIGI detectors exist in gradient masking, we analyze the aggregated gradient convergence properties. We take the adversarial examples crafted by CNNSpot on ProGan as an example. For each plot, we randomly sample 500 adversarial examples generated by a specific attack to compute their expected loss gradients. Each dot shown in Fig. 8 represents a component of the expected loss gradient from each image, in which there are a total of 75k loss gradient components.

Most gradient components of adversarial examples generated by IFGSM (Fig. 8(a)) and MIFGSM (Fig. 8 (c)) tend to stabilize around zero, indicating the vanishing gradient leading to a limited transferability to IFGSM and MIFGSM. Because the only difference between IFGSM and PGD is that PGD randomly chooses the starting point within the l_∞ constraint, we apply random initialization to MIFGSM and find the value of gradient component increase (Fig. 8 (d)), w.r.t. the average success rate increasing from 40.4% to 58.6% (still lower 10.6% than ours). This analysis formally demonstrates the phenomenon of gradient masking in AIGI detectors. Therefore, we advocate for future work for attacks on AIGI detectors to employ randomized-based strategies to circumvent the effect of gradient masking. Our proposed method conducts the spectrum transformation in the frequency domain and hence is also effective for gradient masking.

2) *Evaluation on Deepfake Datasets*: As we mention before, there is a big difference between AIGI detection and Deepfake detection. But we empirically found that FPBA is also effective for face forgery detection. To demonstrate

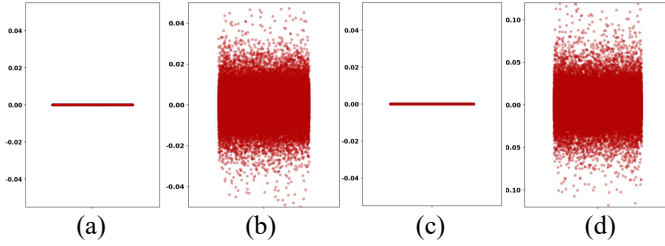


Fig. 8. The gradient components of CNNSpot on adversarial examples generated by different attack methods. (a) gradient components of IFGSM; (b) gradient components of PGD; (c) gradient components of MIFGSM; (d) gradient components of MIFGSM with random initialization.

TABLE XI
ABLATION STUDY ON PROGAN DATASET. THE ADVERSARIAL SAMPLES ARE CRAFTED FROM CNNSPOT.

Attack	DenseNet	MobileNet	Spec	ViT
Spatial	71.5	34.0	27.1	11.0
Frequency	91.0	64.7	36.7	16.9
Spatial-frequency	96.2	66.2	47.9	21.0

TABLE XII
THE ATTACK SUCCESS RATES (%) OF FPBA ON NORMALLY TRAINED DETECTORS W.R.T THE NUMBER N OF SPECTRUM TRANSFORMATIONS. “AVERAGE” WAS CALCULATED AS THE AVERAGE TRANSFER SUCCESS RATE OVER ALL VICTIM MODELS EXCEPT FOR THE SURROGATE MODEL.

N	ResNet	DenNet	EffNet	MobNet	Spec	DCTA	ViT	Swin	Ave.
0	64.5	64.0	37.3	60.6	17.5	48.4	40.5	59.7	48.8
5	98.9	98.0	76.4	95.9	19.8	48.0	51.5	94.8	69.2
10	99.6	99.1	78.6	97.5	19.9	48.0	52.4	96.5	70.3
15	99.4	99.0	78.2	96.6	20.2	48.3	53.0	96.2	70.2
20	99.2	98.7	77.5	96.7	20.7	48.6	51.1	95.6	69.8

this, we conduct the experiments on synthetic FFHQ face datasets [46], which is consist of 50k real face images from FFHQ and 50k fake generated face images created by StyleGAN2 [47]. We report the results in Table IX. Although FPBA is not specific designed for Deepfake detection, it still achieve the best white-box attack performance. For transfer-based attack, FPBA also has the top-2 performance, demonstrating that FPBA is a universal threat across both AIGI and Deepfake detection.

G. Ablation Study

a) Spatial and Frequency Attack: We conduct an ablation study in Table XI to investigate the impact of computing gradient in different domains. In comparison with computing attack gradient solely in the spatial domain or frequency domain, our spatial-frequency attack achieves higher transferability. More ablation studies can be found in the supplementary material.

b) Number (N) of Spectrum Transformations: In this study, we investigate the impacts on the number (N) of spectrum transformations, which can simulate diverse substitute models. The adversarial examples were crafted from ResNet-50 in LSUN(ProGAN) dataset. With the exception of N , other hyper-parameters keep the same with the default settings in the paper. As shown in Table XII, with N increasing 5 from 0, FPBA shows a substantial augmentation in attack success rate. Further, when $N > 5$, there is a diminishing gain in attack success rate but with increased computation. Considering the trade-off between attack performance and computation cost, we set $N = 5$ by default.

V. CONCLUSION

In this paper, we fully investigate the robustness of AIGI detectors against adversarial attacks. For the task of AIGI detection, we propose a novel frequency-based post-train Bayesian attack, which explores the vulnerable regions in the frequency domain in a Bayesian manner. More broadly, our proposed post-train Bayesian attack strategy extends the Bayesian attack family. Extensive experiments have been conducted across models, generators and defense methods under both white-box and black-box settings. The following conclusions can be drawn from our investigation.

- The current SOTA AIGI detectors are vulnerable to adversarial attacks, while the widely-used defense mechanism adversarial training cannot be directly applied to the AIGI detectors, which brings great challenges to build reliable and robust detectors.
- AIGI detectors rely on gradient masking to mitigate the transferability of gradient-based attacks, but the effect of gradient masking can be easily circumvented by a simple random initialization strategy.
- The attack success rate is positively associated with the detection accuracy. Therefore, evaluating detector robustness on low-accuracy subsets is futile, as there are no effective gradients for attack.

These findings indicate that building an adversarial robust AIGI detector is still an open problem. We hope that our work can be used as a protocol to evaluate the robustness of AIGI detectors and draw more attention to this domain.

ACKNOWLEDGMENTS

This work was supported in part by the NSF China (No. 62302139) and FRFCU-HFUT (JZ2023HGTA0202, JZ2023HGQA0101).

REFERENCES

- [1] I. Goodfellow, J. Pouget-Abadie, M. Mirza, B. Xu, D. Warde-Farley, S. Ozair, A. Courville, and Y. Bengio, “Generative adversarial nets,” *NIPS*, vol. 27, 2014.
- [2] J. Ho, A. Jain, and P. Abbeel, “Denoising diffusion probabilistic models,” *NIPS*, vol. 33, pp. 6840–6851, 2020.
- [3] S.-Y. Wang, O. Wang, R. Zhang, A. Owens, and A. A. Efros, “Cnn-generated images are surprisingly easy to spot... for now,” in *CVPR*, 2020, pp. 8695–8704.
- [4] N. Zhong, Y. Xu, Z. Qian, and X. Zhang, “Rich and poor texture contrast: A simple yet effective approach for ai-generated image detection,” *arXiv preprint arXiv:2311.12397*, 2023.
- [5] N. Carlini and H. Farid, “Evading deepfake-image detectors with white- and black-box attacks,” in *CVPR workshops*, 2020, pp. 658–659.
- [6] S. Hussain, P. Neekhara, M. Jere, F. Koushanfar, and J. McAuley, “Adversarial deepfakes: Evaluating vulnerability of deepfake detectors to adversarial examples,” in *WACV*, 2021, pp. 3348–3357.
- [7] P. Neekhara, B. Dolhansky, J. Bitton, and C. C. Ferrer, “Adversarial threats to deepfake detection: A practical perspective,” in *CVPR*, 2021, pp. 923–932.
- [8] Y. Hou, Q. Guo, Y. Huang, X. Xie, L. Ma, and J. Zhao, “Evading deepfake detectors via adversarial statistical consistency,” in *CVPR*, 2023, pp. 12 271–12 280.
- [9] S. Jia, C. Ma, T. Yao, B. Yin, S. Ding, and X. Yang, “Exploring frequency adversarial attacks for face forgery detection,” in *CVPR*, 2022, pp. 4103–4112.
- [10] T. Dzanic, K. Shah, and F. Witherden, “Fourier spectrum discrepancies in deep network generated images,” *NIPS*, vol. 33, pp. 3022–3032, 2020.

- [11] J. Frank, T. Eisenhofer, L. Schönherr, A. Fischer, D. Kolossa, and T. Holz, “Leveraging frequency analysis for deep fake image recognition,” in *ICML*. PMLR, 2020, pp. 3247–3258.
- [12] M. Zhu, H. Chen, Q. Yan, X. Huang, G. Lin, W. Li, Z. Tu, H. Hu, J. Hu, and Y. Wang, “Genimage: A million-scale benchmark for detecting ai-generated image,” *NIPS*, vol. 36, 2024.
- [13] D. P. Kingma and M. Welling, “Auto-encoding variational bayes,” in *ICLR*, Y. Bengio and Y. LeCun, Eds., 2014. [Online]. Available: <http://arxiv.org/abs/1312.6114>
- [14] A. Luo, R. Cai, C. Kong, Y. Ju, X. Kang, J. Huang, and A. C. K. Life, “Forgery-aware adaptive learning with vision transformer for generalized face forgery detection,” *IEEE Transactions on Circuits and Systems for Video Technology*, 2024.
- [15] Y. Yu, X. Zhao, R. Ni, S. Yang, Y. Zhao, and A. C. Kot, “Augmented multi-scale spatiotemporal inconsistency magnifier for generalized deepfake detection,” *IEEE Transactions on Multimedia*, vol. 25, pp. 8487–8498, 2023.
- [16] Z. Guo, G. Yang, J. Chen, and X. Sun, “Exposing deepfake face forgeries with guided residuals,” *IEEE Transactions on Multimedia*, vol. 25, pp. 8458–8470, 2023.
- [17] R. Corvi, D. Cozzolino, G. Zingarini, G. Poggi, K. Nagano, and L. Verdoliva, “On the detection of synthetic images generated by diffusion models,” in *ICASSP*. IEEE, 2023, pp. 1–5.
- [18] X. Zhang, S. Karaman, and S.-F. Chang, “Detecting and simulating artifacts in gan fake images,” in *2019 IEEE international workshop on information forensics and security (WIFS)*. IEEE, 2019, pp. 1–6.
- [19] Y. Ju, S. Jia, J. Cai, H. Guan, and S. Lyu, “Giff: Global and local feature fusion for ai-synthesized image detection,” *IEEE Transactions on Multimedia*, 2023.
- [20] P. Lorenz, R. L. Durall, and J. Keuper, “Detecting images generated by deep diffusion models using their local intrinsic dimensionality,” in *ICCV*, 2023, pp. 448–459.
- [21] Y. Jeong, D. Kim, Y. Ro, P. Kim, and J. Choi, “Fingerprintnet: Synthesized fingerprints for generated image detection,” in *ECCV*. Springer, 2022, pp. 76–94.
- [22] B. Liu, F. Yang, X. Bi, B. Xiao, W. Li, and X. Gao, “Detecting generated images by real images,” in *ECCV*. Springer, 2022, pp. 95–110.
- [23] C. Tan, Y. Zhao, S. Wei, G. Gu, and Y. Wei, “Learning on gradients: Generalized artifacts representation for gan-generated images detection,” in *CVPR*, 2023, pp. 12 105–12 114.
- [24] U. Ojha, Y. Li, and Y. J. Lee, “Towards universal fake image detectors that generalize across generative models,” in *CVPR*, 2023, pp. 24 480–24 489.
- [25] Z. Wang, J. Bao, W. Zhou, W. Wang, H. Hu, H. Chen, and H. Li, “Dire for diffusion-generated image detection,” in *ICCV*, 2023, pp. 22 445–22 455.
- [26] J. Ricker, D. Lukovnikov, and A. Fischer, “Aeroblade: Training-free detection of latent diffusion images using autoencoder reconstruction error,” *arXiv preprint arXiv:2401.17879*, 2024.
- [27] M. Zhu, H. Chen, M. Huang, W. Li, H. Hu, J. Hu, and Y. Wang, “Gendet: Towards good generalizations for ai-generated image detection,” *arXiv preprint arXiv:2312.08880*, 2023.
- [28] Y. Zhang and X. Xu, “Diffusion noise feature: Accurate and fast generated image detection,” *arXiv preprint arXiv:2312.02625*, 2023.
- [29] Z. Zhao, Z. Liu, and M. Larson, “Adversarial image color transformations in explicit color filter space,” *IEEE Transactions on Information Forensics and Security*, vol. 18, pp. 3185–3197, 2023.
- [30] R. Ran, J. Wei, C. Zhang, G. Wang, Y. Yang, and H. T. Shen, “Adaptive multi-scale degradation-based attack for boosting the adversarial transferability,” *IEEE Transactions on Multimedia*, 2024.
- [31] D. Gao, L. Ou, Y. Liu, Q. Yang, and H. Wang, “Deepspooof: Deep reinforcement learning-based spoofing attack in cross-technology multimedia communication,” *IEEE Transactions on Multimedia*, 2024.
- [32] Y. Diao, T. Shao, Y.-L. Yang, K. Zhou, and H. Wang, “Basar: black-box attack on skeletal action recognition,” in *CVPR*, 2021, pp. 7597–7607.
- [33] A. Kurakin, I. J. Goodfellow, and S. Bengio, “Adversarial examples in the physical world,” in *Artificial intelligence safety and security*. Chapman and Hall/CRC, 2018, pp. 99–112.
- [34] I. J. Goodfellow, J. Shlens, and C. Szegedy, “Explaining and harnessing adversarial examples,” *arXiv preprint arXiv:1412.6572*, 2014.
- [35] D. Li, W. Wang, H. Fan, and J. Dong, “Exploring adversarial fake images on face manifold,” in *CVPR*, 2021, pp. 5789–5798.
- [36] Y. Huang, F. Juefei-Xu, R. Wang, Q. Guo, L. Ma, X. Xie, J. Li, W. Miao, Y. Liu, and G. Pu, “Fakepolisher: Making deepfakes more detection-evasive by shallow reconstruction,” in *ACM MM*, 2020, pp. 1217–1226.
- [37] M. Wu, J. Ma, R. Wang, S. Zhang, Z. Liang, B. Li, C. Lin, L. Fang, and L. Wang, “Tracevader: Making deepfakes more untraceable via evading the forgery model attribution,” in *AAAI*, vol. 38, no. 18, 2024, pp. 19 965–19 973.
- [38] A. Madry, A. Makelov, L. Schmidt, D. Tsipras, and A. Vladu, “Towards deep learning models resistant to adversarial attacks,” *arXiv preprint arXiv:1706.06083*, 2017.
- [39] Y. Long, Q. Zhang, B. Zeng, L. Gao, X. Liu, J. Zhang, and J. Song, “Frequency domain model augmentation for adversarial attack,” in *ECCV*. Springer, 2022, pp. 549–566.
- [40] P. Izmailov, S. Vikram, M. D. Hoffman, and A. G. G. Wilson, “What are bayesian neural network posteriors really like?” in *ICML*. PMLR, 2021, pp. 4629–4640.
- [41] Y. He, B. Gan, S. Chen, Y. Zhou, G. Yin, L. Song, L. Sheng, J. Shao, and Z. Liu, “Forgerynet: A versatile benchmark for comprehensive forgery analysis,” in *CVPR*, 2021, pp. 4360–4369.
- [42] J. T. Springenberg, A. Klein, S. Falkner, and F. Hutter, “Bayesian optimization with robust bayesian neural networks,” vol. 29, 2016.
- [43] T. Karras, T. Aila, S. Laine, and J. Lehtinen, “Progressive growing of gans for improved quality, stability, and variation,” in *ICLR*, 2018.
- [44] J. Deng, W. Dong, R. Socher, L.-J. Li, K. Li, and L. Fei-Fei, “Imagenet: A large-scale hierarchical image database,” in *CVPR*. Ieee, 2009, pp. 248–255.
- [45] R. Rombach, A. Blattmann, D. Lorenz, P. Esser, and B. Ommer, “High-resolution image synthesis with latent diffusion models,” in *CVPR*, 2022, pp. 10 684–10 695.
- [46] F. Shamshad, K. Srivatsan, and K. Nandakumar, “Evading forensic classifiers with attribute-conditioned adversarial faces,” in *CVPR*, 2023, pp. 16 469–16 478.
- [47] T. Karras, S. Laine, and T. Aila, “A style-based generator architecture for generative adversarial networks,” in *CVPR*, 2019, pp. 4401–4410.
- [48] A. G. Howard, M. Zhu, B. Chen, D. Kalenichenko, W. Wang, T. Weyand, M. Andreetto, and H. Adam, “Mobilenets: Efficient convolutional neural networks for mobile vision applications,” *arXiv preprint arXiv:1704.04861*, 2017.
- [49] M. Tan and Q. Le, “Efficientnet: Rethinking model scaling for convolutional neural networks,” in *ICML*. PMLR, 2019, pp. 6105–6114.
- [50] G. Huang, Z. Liu, L. Van Der Maaten, and K. Q. Weinberger, “Densely connected convolutional networks,” in *CVPR*, 2017, pp. 4700–4708.
- [51] A. Dosovitskiy, L. Beyer, A. Kolesnikov, D. Weissenborn, X. Zhai, T. Unterthiner, M. Dehghani, M. Minderer, G. Heigold, S. Gelly *et al.*, “An image is worth 16x16 words: Transformers for image recognition at scale,” *arXiv preprint arXiv:2010.11929*, 2020.
- [52] Z. Liu, Y. Lin, Y. Cao, H. Hu, Y. Wei, Z. Zhang, S. Lin, and B. Guo, “Swin transformer: Hierarchical vision transformer using shifted windows,” in *ICCV*, 2021, pp. 10 012–10 022.
- [53] Z. Liu, X. Qi, and P. H. Torr, “Global texture enhancement for fake face detection in the wild,” in *CVPR*, 2020, pp. 8060–8069.
- [54] Y. Dong, F. Liao, T. Pang, H. Su, J. Zhu, X. Hu, and J. Li, “Boosting adversarial attacks with momentum,” in *CVPR*, 2018, pp. 9185–9193.
- [55] C. Luo, Q. Lin, W. Xie, B. Wu, J. Xie, and L. Shen, “Frequency-driven imperceptible adversarial attack on semantic similarity,” in *CVPR*, 2022, pp. 15 315–15 324.
- [56] Y. Xiong, J. Lin, M. Zhang, J. E. Hopcroft, and K. He, “Stochastic variance reduced ensemble adversarial attack for boosting the adversarial transferability,” in *CVPR*, 2022, pp. 14 983–14 992.
- [57] H. Wang, Y. Diao, Z. Tan, and G. Guo, “Defending black-box skeleton-based human activity classifiers,” in *AAAI*, vol. 37, no. 2, 2023, pp. 2546–2554.
- [58] A. Radford, J. W. Kim, C. Hallacy, A. Ramesh, G. Goh, S. Agarwal, G. Sastry, A. Askell, P. Mishkin, J. Clark *et al.*, “Learning transferable visual models from natural language supervision,” in *ICML*. PMLR, 2021, pp. 8748–8763.
- [59] Midjourney, “<https://www.midjourney.com/home/>,” 2022.
- [60] P. Dhariwal and A. Nichol, “Diffusion models beat gans on image synthesis,” *NIPS*, vol. 34, pp. 8780–8794, 2021.
- [61] Wukong, “<https://xihe.mindspore.cn/modelzoo/wukong>,” 2022.
- [62] A. Brock, J. Donahue, and K. Simonyan, “Large scale gan training for high fidelity natural image synthesis,” in *ICLR*, 2018.
- [63] A. Athalye, N. Carlini, and D. Wagner, “Obfuscated gradients give a false sense of security: Circumventing defenses to adversarial examples,” in *ICML*. PMLR, 2018, pp. 274–283.